CORC® Cables: Numerical Characterization of the Critical Current After Bending

CORC Cables: Numerical Characterization of the Critical Current After Bending

S. Viarengo, *Student Member, IEEE*, F. Freschi, *Senior Member, IEEE*, and L. Savoldi, *Member, IEEE*

***Abstract*—To satisfy requirements of high operating current densities, compact layouts, and the possibility to reach magnetic field higher than 20 T, at temperatures from 4.2 K to 20 K, e.g., necessary for the development of next generation of colliders, the CORC® cable concept is of particular interest. Based on ReBCO high temperature superconducting tapes wound around a copper former, it exploits round cross-section guaranteeing electrical and mechanical isotropy. However, these cables can degrade as a result of the winding process and operating conditions, as ReBCO tapes are strain-sensitive. This paper presents a 3D multiphysics numerical model for characterizing the critical current (I_c) of bended ReBCO CORC® cables, based on a *T–A* formulation implemented in COMSOL Multiphysics® coupled with a thermal model of a straight cable, already validated against experimental results. The tape is approximated as a thin shell, taking advantage of its high aspect ratio, and the I_c scaling for the tape accounts for the local strain. A pure geometrical strain evaluation on the tape surface allow to properly account for the punctual degradation of I_c, as an input for the multi-physics model. The assessment of the voltage-current curve for the bent conductor has been compared to experimental results.**

***Index Terms*—CORC cable, critical current, HTS, multiphysics model, ReBCO , strain.**

I. Introduction

In THE framework of future generation of particle accelerators, the next frontier is reaching magnetic field up to 20 T [1]. High temperature superconductors (HTS) allow the possibility to reach those high fields [2], guaranteeing at the same time high electrical performances and high thermal stability. Both bismuth strontium calcium copper oxide, BSCCO, strands [3] and ReBCO tapes [4] are under investigation for future dipole magnets [5], [6]. The high elasticity of yttrium barium copper oxide (YBCO) and the tape strength increased by the hastelloy (see Fig. 1(b)) led to the development of the conductor in round core (CORC®) cable [7]. Several layers of YBCO tapes are helically wounded in opposite winding directions on a copper core allowing a high current density [8], an isotropy flexibility and mechanical strength, with a reduction of AC losses [9], [10], [11]. As the critical current I_c of ReBCO tapes are strain sensitive, the bending fabrication and winding of the coil degrade the cable performances [12], [13]. Numerical models capable to predict the cable performance should proceed along with experimental characterization. Some analytical solution for the strain prediction on a tape are present in literature: in [14], a curvature-based model provided analytical formulas for strain computation for different bending modes, without taking into account local deformation due to the Poisson's effect. In [15], a parametric analysis for different bending radii were performed numerical and analytically based on Flexure formula. In [16], [17] and [18], structural finite element analyses were used to investigate the mechanical strain generated in tapes with different winding angles: the studies showed that compression decreases towards the edge along the tape width. A combined tension and torsion analysis is carried out in [19]. Regarding the CORC® cable, in [20] a 3D mechanical simulation computed the strain distribution on tapes, after winding and bending processes, to compare results with critical current and AC losses measurements on a 6-layer CORC® coil built from authors. In [8] a detailed parametric analysis, validated through experiments, aimed at defining the stress-strain state for the determination of the critical strain that may cause the breakage of the YBCO layer, considering the bending of the cable. In [21] and in [22], electromechanical simulation, based on *T–A* formulation, were performed to predict the strain state and the critical current degradation for straight CORC® cables. The thermal behavior was not considered in those models and the current was imposed without any possibility of redistributing, if necessary, due to uneven strain in different tapes. In this paper,

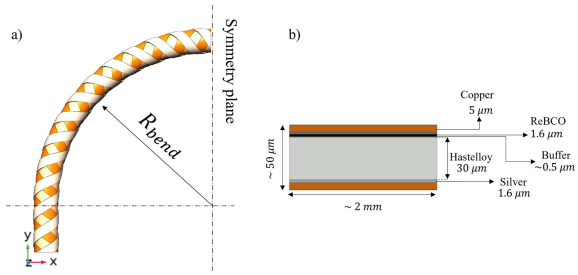

Fig. 1. Cable layout (a) and tape (b) considered in this study.

Manuscript received 26 September 2023; revised 20 November 2023; accepted 15 December 2023. Date of publication 1 January 2024; date of current version 19 January 2024. This work was supported by the EUROfusion Consortium, funded by the European Union via the Euratom Research and Training Programme under Grant 101052200– EUROfusion. *(Corresponding author: S. Viarengo.)*

S. Viarengo and L. Savoldi are with the Dipartimento Energia 'Galileo Ferraris', Politecnico di Torino, 10139 Torino, Italy (e-mail: sofia.viarengo@polito.it; laura.savoldi@polito.it).

F. Freschi is with the Dipartimento Energia 'Galileo Ferraris', Politecnico di Torino, 10139 Torino, Italy, and also with the School of Information Technology and Electrical Engineering, University of Queensland, Brisbane, QLD 4072, Australia (e-mail: fabio.freschi@polito.it).

Color versions of one or more figures in this article are available at https://doi.org/10.1109/TASC.2023.3348090.

Digital Object Identifier 10.1109/TASC.2023.3348090

a 3D multiphysics model in COMSOL Multiphysics®, based on the *T–A* formulation, is proposed for bended CORC® cables along with a simplified evaluation of the strain, based on pure geometrical assumptions. The strain map allows to determine the I_c degradation due to the deformation in each element of the computational domain. The model is coupled to a thermal module and aims at the prediction of the cable I_c and $V-I$ curve. A specific boundary condition allows the redistribution of the current among tapes and layers according to the temperature, strain, and magnetic field maps. In Section II, tapes, cable layout and material properties are reported.

II. YBCO Tapes and Cable Layout

The CORC® considered in this work has a 6-tapes, three layers and two tapes per layer, see Fig. 1(a), with a length of $405\,\mathrm{mm}$ and $20\,\mathrm{mm}$ of bending radius. The core diameter is $2.8\,\mathrm{mm}$ and the twist pitch $5.7\,\mathrm{mm}$. The tapes of SuperPower Inc. [23] made of YBCO are the one considered in this study, with the geometrical parameters reported in Fig. 1(b). The multi-material tape thickness is treated as an homogenized material: the thermophysical properties of each material were taken from [24]. The density was weighted on the cross section, while the specific heat on the mass. The thermal conductivity is anisotropic: along the direction parallel to the tape surface, thermal resistances are arranged in parallel, whereas resistances are arranged in series along the perpendicular direction. The equivalent electric conductivity σ_{eq} is computed as a parallel among layers weighted on the cross section:

$$\sigma_{eq} = \frac{\sum_{i=1}^{N_l} \sigma_i A_i}{\sum_{i=1}^{N_l} A_i} \tag{1}$$

where σ_i are the electric conductivities of the layers (the subscript i is referred to the ith layer), taken from [24], A_i are the cross sections and N_l is the number of layers within the tape. The YBCO electric conductivity is computed from the power law in (2):

$$\sigma_{YBCO} = \frac{J_c\left(B_\parallel, B_\perp, \theta, \varepsilon\right)}{E_0}\left(\frac{J}{J_c\left(B_\parallel, B_\perp, \theta, \varepsilon\right)}\right)^{1-n} \tag{2}$$

where E_0 is the critical field set to $1\,\mu\mathrm{V/cm}$, J is the current density flowing in the superconductor, n is the power law exponent, and J_c is the critical current density. The J_c is dependent on the temperature θ, magnetic field B and the strain ε [25], [26], according to:

$$J_c\left(B_\parallel, B_\perp, \theta, \varepsilon\right) = \psi(\varepsilon) J_{c0}\left(\frac{\theta_{c0}-\theta}{\theta_{c0}-\theta_0}\right)\frac{1}{\left[1+\frac{\sqrt{\left(kB_\parallel\right)^2+B_\perp^2}}{B_c}\right]^b} \tag{3}$$

Where J_{c0} is the critical current density at zero field, θ_{c0} is the critical temperature, θ_0 is the operating temperature, θ is the temperature of the superconductor. The fitting parameter at 77 K for the cable under study are taken from [27] and reported in Table I. The $\psi(\varepsilon) = I_c/I_{c0}$ parameter represents the critical current degradation due to the strain: the strain evaluation is reported in the next section and the value of ψ is taken from [28].

TABLE I
J_c Characterization: Fitting Parameters for a Single Tape (from [27])

Parameters	Value	Units
θ_0	77	K
J_{c0}	2.6×10^{10}	$\mathrm{A/m^2}$
θ_{c0}	93	K
k	0.275	–
B_c	100	mT
b	0.25	–
n	22	–

III. Numerical Model

Taking advantage of the high aspect ratio on ReBCO tape, the *T–A* formulation [29] has been implemented in COMSOL Multiphysics® and suitably coupled with a thermal module to account for heat transfer in a shell.. Under magneto quasi-static approximation, the model is based on two potentials: the current vector potential $\mathbf{T}$ for the conducting solved for shell domain, and the magnetic vector potential $\mathbf{A}$ solved for the whole domain. Since the tape is a shell, the current only flows along its tangential direction and it is supposed to be uniform along the width, neglecting the component orthogonal to the surface. $\mathbf{T}$ is considered perpendicular to the shell surface and the current density $\mathbf{J}$ is computed as the curl of $\mathbf{T}$. The $\mathbf{A}$ is defined over the entire computational domain, and the magnetic flux density $\mathbf{B}$ is computed as the curl of $\mathbf{A}$. The final governing are:

$$\nabla\times\left[\frac{1}{\sigma_{eq}}\nabla\times T\mathbf{n}\right]\cdot\mathbf{n} = -\frac{\partial\mathbf{B}}{\partial t}\cdot\mathbf{n} \tag{4}$$

$$\nabla\times\left(\frac{1}{\mu}\nabla\times\mathbf{A}\right) = \mathbf{J} \tag{5}$$

Where μ is the vacuum permeability, T is a scalar and $\mathbf{n}$ is the normal to the shell surface. The current redistribution are is guaranteed through the application of a specific boundary condition reported in [27]. For the thermal module, the heat conduction equation is solved for the tape domain:

$$\rho_{eq}C_{eq}\frac{\partial\boldsymbol{\theta}}{\partial t} = -\nabla\cdot\left(\lambda_{eq}\left(\theta\right)\nabla\theta\right) + \dot{q}\left(\theta\right) \tag{6}$$

Where ρ_{eq} is the homogenized density, C_{eq} is the homogenized specific heat, λ_{eq} is the homogenized thermal conductivity, and θ is the temperature. The source term $\dot{q}$ is given by the sum of three contributions: the joule losses, if any, the conduction among overlapping tapes, and the cooling from the LN_2 bath. Further informations about the multiphysics model are reported in [27].

IV. Strain Evaluation

In this work, no mechanical analysis has been carried out, but the map of strain has been extrapolated both from literature and from some simplified geometrical assumptions based on

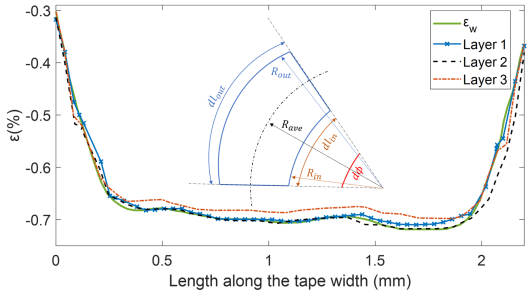

Fig. 2. Intrinsic strain distribution of the tape from [17] and final total distributions along the width at the cable center cross section. Inset: sketch of an element after bending, for strain evaluation.

the definition of strain (the ratio among the elongation ΔL and the initial length L_0). Three strain contributions have been considered:

- intrinsic strain due to the winding of the tape on the copper core ε_w;
- strain due to the bending ε_b;
- shrinkage of the tape due to the bending ε_s.

A. Winding of an Individual Tape

In the CORC® cable design, tapes are helically wound around the central copper core inducing local deformation. The ReBCO layer is above the neutral plane, so it will be in compression state [14]. The non-uniform longitudinal strain distribution along the width ε_w, computed in [17], has been imposed on each tape, see Fig. 2.

B. Cable Bending

After the bending process, part of the cable above the neutral radius R_{ave} is in tension state, while the one below it is in compression (see Fig. 3(a)). Based on strain definition:

$$\varepsilon_{out} = \frac{R_{out} - R_{ave}}{R_{ave}} \tag{7}$$

$$\varepsilon_{in} = \frac{R_{in} - R_{ave}}{R_{ave}} \tag{8}$$

where subscripts out and in are referred to the part above and below the neutral radius, respectively. Generalizing, the strain along all the cable is computed as:

$$\varepsilon_b = \frac{R - R_{ave}}{R_{ave}} \tag{9}$$

Where R is the cylindrical coordinate, see Fig. 2.

C. Tape Shrinkage Due to Bending

The tension state led to a shrinkage of the tape, that has been considered in this study, see Fig. 3(a). Based on the volume conservation, the final thickness is computed as:

$$V_{tape} = R_{ave}^2 \phi t \tag{10}$$

$$t_{fin} = \frac{V_{tape}}{R_{ave} R \phi} \tag{11}$$

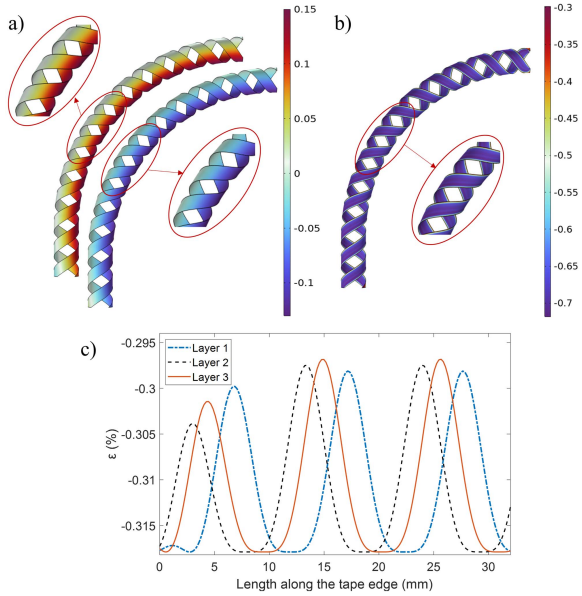

Fig. 3. Strain maps: a) tension compression (top) and shrinkage (bottom) due to bending process; b) total strain map. c) Total strain distributions along the first 32 mm of the tape edges (3 subsequent pitches).

Where V_{tape} is the tape volume, ϕ is the angular coordinate of the cylindrical system (see Fig. 2), t is the thickness, and the subscript $_{fin}$ is referred to after bending process. Therefore, the strain ε_s is:

$$\varepsilon_s = \frac{t_{fin} - t_{init}}{t_{init}} \tag{12}$$

Where t_{init} is the initial thickness of the tape.

D. Total Strain

The total strain ε is computed by the superposition principle:

$$\varepsilon = \varepsilon_w + \varepsilon_b + \varepsilon_s \tag{13}$$

Fig. 2 shows the strain distribution along the tape width of the three layers. Fig. 3(b) and (c) report the total strain map and distribution along the tape edges. From Fig. 3(c), it possible to notice the increase of the average strain value from the straight part of the cable to the bended one, and the periodic behaviour among subsequent pitches. The percentage of degradation $\psi(\varepsilon)$ of the tape critical current density due to the strain state has been extrapolated from [28].

V. Validation of the Model

The results of the proposed model have been compared to the experimental results, measured on a bended 6-tapes CORC® cable tested at the Lawrence Berkeley National Laboratory (LBNL). The $V - I$ curve is measured in a LN_2 bath at 77 K and in self-field conditions.

A. Experimental Setup

The sketch of the experimental setup is reported in Fig. 4(a). Details can be found in [30]. Different bending radii and vacuum pressure impregnation procedures were performed to quantify

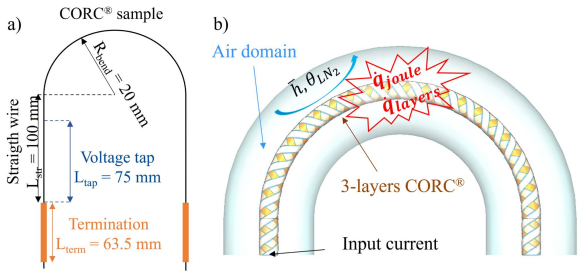

Fig. 4. Sketch of a) the experimental setup and b) the simulated domain and boundary conditions.

the degradation of cable performances. In this study, the Sample 2b of [30] is considered. The wire was bended in an aluminum fixture in grooves of $4.5\,\mathrm{mm}$ diameter. Voltage taps were soldered to the wires at distances 5, 40 and $75\,\mathrm{mm}$ up from the bottom of the copper terminations. Tapered tapes in the terminations had been soldered to the copper tube to guarantee a proper current injection.

B. Model Setup

In the cable model, an environment temperature of $77\,\mathrm{K}$ is considered, the current is ramped up, and the voltage drop is computed once the steady-state condition is reached. The domain and the boundary conditions are sketched in Fig. 4(b). The straight part as been simulated separately: leveraging on the periodicity of the geometry, just a pitch has been considered. The curved part has been simulated considering a pitch to avoid edge effects. The voltage drop V_{tot} has computed by the sum of voltages drop on the two domains:

$$V_{tot} = \int_{L_{str}} \mathbf{E}_{str} \cdot \mathrm{dl} + \int_{L_{curve}} \mathbf{E}_{curve} \cdot \mathrm{dl} \qquad (14)$$

Where L is the cable length, E is the electric field, subscripts str and $curve$ are referred to the straight and the curve part, respectively. The mesh counts about $640\mathrm{k}$ elements with an average quality of 0.6. The simulation of a single value of current might run for $\sim 1\,\mathrm{h}$, when the current density is far from the critical condition. In the latter case, it requires $\sim 6.5\,\mathrm{h}$.

C. $V - I$ Results

Fig. 5(a) reports the comparison between the measurements and the numerical model of the $V - I$ curve, as well as the critical current. The critical current value is well-captured from the model: the measured I_c is $\sim 218\,\mathrm{A}$, while the computed is $\sim 217\,\mathrm{A}$. Nonetheless, the total performance of the cable, specifically the n-value is largely overestimated in COMSOL. The measured n-value is ~ 6.5, while the computed is ~ 15. The main possible reason for this behavior is that since the cable is short, the termination may still play a significant role in the voltage drop. Moreover, a better strain evaluation through a proper mechanical model, which considers buckling of tapes, might explain this discrepancy. In Fig. 5(b), the average electric field of the bended part E_{bended} and of a straight pitch $E_{straight}$ are compared: as expected, the E_{bended} is higher due to the stronger deformation. The temperature increases about $\sim 10\,\mathrm{mK}$

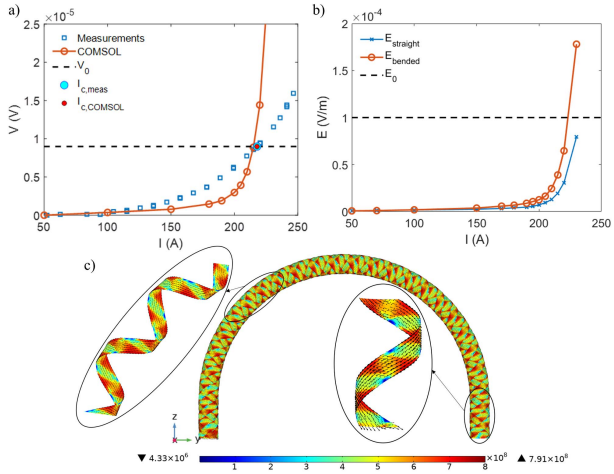

Fig. 5. (a) Comparison between measured and numerically computed $V - I$ curves. Square dots referred to the experimental data, red solid line to the COMSOL simulation, the light blue circle is the measured I_c, and finally the red dot is the COMSOL I_c. (b) Comparison between the average electric field of the bended part, red line, and of a straight pitch, blue line. (c) Current density map at 150 A of total input current.

when the current reaches the I_c, and it can rise of about $30\,\mathrm{mK}$ at $230\,\mathrm{A}$ (when the tape transits to the normal state). In Fig. 5(c), the norm of the current density distribution J_{norm} in self-field is shown. The total input current is $150\,\mathrm{A}$ (each tape experiences $\sim 0.5 I_c$), so the tapes are fully in the superconductive state. The non-homogenous distribution of the current density is due to the self-induced magnetic field among different tapes. The magnetic field is stronger on the outermost layer and where tapes overlap, with a consequent reduction of the critical current density, increase of the resistivity, and therefore the redistribution of the current.

VI. Conclusion

In this work, a full 3D magneto-thermal model of a bended CORC® cable is developed for the first time in COMSOL Multiphysics®, relying on a *T–A* formulation. A pure geometrical evaluation of strain allows the degradation of the I_c. The $V - I$ curve computed by the model has been to reproduce a test at LBNL of a 6-tape CORC® wire, in self-field immersed in LN_2 bath: the critical current has been well-capture, but the n-value is largely overestimated. The main reasons might be a strong influence of the termination, since it is a short cable, and the strong simplification of the strain state. In perspective, the CORC® model would be validated through available data in literature and coupled to a mechanical module. Finally, it will extend to more than 3-layer CORC® , other layouts and different external conditions.

Acknowledgment

Views and opinions expressed are however those of the author(s) only and do not necessarily reflect those of the European Union, or the European Commission. Neither the European Union nor the European Commission can be held responsible for them. The authors acknowledge X. Wang from LBNL for sharing measurements data and expertise about CORC® cable design and behavior.

REFERENCES

[1] L. Rossi et al., "The EuCARD-2 future magnets European collaboration for accelerator-quality HTS magnets," *IEEE Trans. Appl. Supercond.*, vol. 25, no. 3, Jun. 2015, Art. no. 4001007.

[2] D. C. Larbalestier et al., "Isotropic round-wire multifilament cuprate superconductor for generation of magnetic fields above 30 T," *Nature Mater.*, vol. 13, no. 4, pp. 375–381, Apr. 2014.

[3] K. Heine, J. Tenbrink, and M. Thöner, "High-field critical current densities in $Bi_2Sr_2Ca_1Cu_2O_{8+X}$/Ag wires," *Appl. Phys. Lett.*, vol. 55, no. 23, pp. 2441–2443, Dec. 1989.

[4] A. K. Jha and K. Matsumoto, "Superconductive REBCO thin films and their nanocomposites: The role of rare-earth oxides in promoting sustainable energy," *Front. Phys.*, vol. 7, Jun. 2019, Art. no. 82.

[5] L. G. Fajardo et al., "First demonstration of high current canted-cosine-theta coils with Bi-2212 Rutherford cables," *Supercond. Sci. Technol.*, vol. 34, no. 2, Feb. 2021, Art. no. 024001.

[6] J. van Nugteren, G. Kirby, J. Murtomaki, G. DeRijk, L. Rossi, and A. Stenvall, "Toward REBCO 20 T+ dipoles for accelerators," *IEEE Trans. Appl. Supercond.*, vol. 28, no. 4, Jun. 2018, Art. no. 4008509.

[7] D. C. van der Laan, "$YBa_2Cu_3O_{7-\delta}$ coated conductor cabling for low AC-loss and high-field magnet applications," *Supercond. Sci. Technol.*, vol. 22, no. 6, Jun. 2009, Art. no. 065013.

[8] V. A. Anvar et al., "Bending of CORC® cables and wires: Finite element parametric study and experimental validation," *Supercond. Sci. Technol.*, vol. 31, no. 11, Nov. 2018, Art. no. 115006.

[9] J. D. Weiss, T. Mulder, H. J. ten Kate, and D. C. van der Laan, "Introduction of CORC® wires: Highly flexible, round high-temperature superconducting wires for magnet and power transmission applications," *Supercond. Sci. Technol.*, vol. 30, no. 1, Jan. 2017, Art. no. 014002.

[10] G. Xiao et al., "Performance of highly flexible sub-cable for REBCO cable-in-conduit conductor at 5.8 T applied field," *Superconductivity*, vol. 3, Sep. 2022, Art. no. 100023.

[11] J. Zhao et al., "Effect of winding methods: Transport AC losses in CORC coils," *Supercond. Sci. Technol.*, vol. 35, no. 11, Nov. 2022, Art. no. 115007.

[12] P. Gao, J. Mao, J. Chen, X. Wang, and Y. Zhou, "Electromechanical degradation of REBCO coated conductor tapes under combined tension and torsion loading," *Int. J. Mech. Sci.*, vol. 223, Jun. 2022, Art. no. 107314.

[13] K. Ilin et al., "Experiments and FE modeling of stress–strain state in ReBCO tape under tensile, torsional and transverse load," *Supercond. Sci. Technol.*, vol. 28, no. 5, May 2015, Art. no. 055006.

[14] X. Wang, D. Arbelaez, S. Caspi, S. O. Prestemon, G. Sabbi, and T. Shen, "Strain distribution in REBCO-coated conductors bent with the constant-perimeter geometry," *IEEE Trans. Appl. Supercond.*, vol. 27, no. 8, Dec. 2017, Art. no. 6604010.

[15] A. Kb, R. J. Thomas, J. P. Mathai, and A. Nijhuis, "Analytical and numerical investigations on the degradation of REBCO based superconducting tapes under bending," *IEEE Trans. Appl. Supercond.*, vol. 31, no. 7, Oct. 2021, Art. no. 8400712.

[16] K. Wang, W. Ta, and Y. Gao, "The winding mechanical behavior of conductor on round core cables," *Physica C: Supercond. Appl.*, vol. 553, pp. 65–71, Oct. 2018.

[17] F. Pierro et al., "Finite-element analysis of the strain distribution due to bending in a REBCO coated conductor for canted cosine theta dipole magnet applications," *IEEE Trans. Appl. Supercond.*, vol. 29, no. 5, Aug. 2019, Art. no. 4600705.

[18] K. Ashok, R. Thomas, M. J. Prakash, and A. Nijhuis, "Performance limits in REBCO tape for variation in winding parameters of CORC® cable and wire," *Physica C: Supercond. Appl.*, vol. 582, Mar. 2021, Art. no. 1353828.

[19] A. Kb, R. J. Thomas, J. P. Mathai, and A. Nijhuis, "Influence of combined tension and torsion on the performance of REBCO superconducting tapes," *IEEE Trans. Appl. Supercond.*, vol. 33, no. 3, Apr. 2023, Art. no. 7500211.

[20] S. Y. Gao et al., "HTS conductor coil by in-situ winding technology for large-scale high-field magnet," *Supercond. Sci. Technol.*, vol. 36, no. 11, Nov. 2023, Art. no. 115029.

[21] J. Yan, K. Wang, Y. Gao, Y. Zhou, and A. Nijhuis, "Investigating the effect of transverse compressive loads on the electromagnetic performance of superconducting CORC® cables," *Supercond. Sci. Technol.*, vol. 35, no. 11, Nov. 2022, Art. no. 115006. [Online]. Available: https://iopscience.iop.org/article/10.1088/1361-6668/ac9559

[22] K. Wang et al., "Prediction of strain, inter-layer interaction and critical current in CORC® wires under axial strain by T-A modeling," *Supercond. Sci. Technol.*, vol. 35, no. 10, Oct. 2022, Art. no. 105012.

[23] "Home page SuperPower," 2023. [Online]. Available: https://www.superpower-inc.com/

[24] M. Casali, M. Breschi, and P. L. Ribani, "Two-dimensional anisotropic model of YBCO coated conductors," *IEEE Trans. Appl. Supercond.*, vol. 25, no. 1, Feb. 2015, Art. no. 6600112.

[25] B. C. Robert, M. U. Fareed, and H. S. Ruiz, "How to choose the superconducting material law for the modelling of 2G-HTS coils," *Materials*, vol. 12, no. 17, Aug. 2019, Art. no. 2679.

[26] F. Grilli, F. Sirois, V. M. R. Zermeno, and M. Vojenciak, "Self-consistent modeling of the IC of HTS devices: How accurate do models really need to be?," *IEEE Trans. Appl. Supercond.*, vol. 24, no. 6, Dec. 2014, Art. no. 8000508.

[27] S. Viarengo et al., "A new coupled electrodynamic T–A and thermal model for the critical current characterization of high-temperature superconducting Tapes and Cables," *IEEE Access*, vol. 11, pp. 107548–107561, 2023.

[28] D. C. van der Laan, J. D. Weiss, and D. M. McRae, "Status of CORC® cables and wires for use in high-field magnets and power systems a decade after their introduction," *Supercond. Sci. Technol.*, vol. 32, no. 3, Mar. 2019, Art. no. 033001.

[29] H. Zhang, M. Zhang, and W. Yuan, "An efficient 3D finite element method model based on the T–A formulation for superconducting coated conductors," *Supercond. Sci. Technol.*, vol. 30, no. 2, Feb. 2017, Art. no. 024005.

[30] J. Stern et al., "Developing a vacuum pressure impregnation procedure for CORC wires," *IEEE Trans. Appl. Supercond.*, vol. 32, no. 6, Sep. 2022, Art. no. 4800904.

Open Access funding provided by 'Politecnico di Torino' within the CRUI CARE Agreement